Tectonophysics 726 (2018) 137–146

Contents lists available at ScienceDirect

Tectonophysics

journal homepage: www.elsevier.com/locate/tecto

Numerical investigation of deep-crust behavior under lithospheric extension

Megan Korchinski[a,*], Patrice F. Rey[b], Luke Mondy[b], Christian Teyssier[a], Donna L. Whitney[a]

[a] Department of Earth Sciences, University of Minnesota, Minneapolis, MN, USA
[b] EarthByte, School of Geosciences, University of Sydney, Sydney, Australia

ARTICLE INFO

Keywords:
Gneiss domes
Exhumation
Extension
Numerical modeling
Rheology

ABSTRACT

What are the conditions under which lithospheric extension drives exhumation of the deep orogenic crust during the formation of gneiss domes? The mechanical link between extension of shallow crust and flow of deep crust is investigated using two-dimensional numerical experiments of lithospheric extension in which the crust is 60 km thick and the deep-crust viscosity and density parameter space is explored. Results indicate that the style of extension of the shallow crust and the path, magnitude, and rate of flow of deep crust are dynamically linked through the deep-crust viscosity, with density playing an important role in experiments with a high-viscosity deep crust. Three main groups of domes are defined based on their mechanisms of exhumation across the viscosity-density parameter space. In the first group (low-viscosity, low-density deep crust), domes develop by lateral and upward flow of the deep crust at km m.y^{-1} velocity rates (i.e. rate of experiment boundary extension). In this case, extension in the shallow crust is localized on a single interface, and the deep crust traverses the entire thickness of the crust to the Earth's near-surface in 5 m.y. This high exhuming power relies on the dynamic feedback between the flow of deep crust and the localization of extension in the shallow crust. The second group (intermediate-viscosity, low-density deep crust) has less exhuming power because the stronger deep crust flows less readily and instead accommodates more uniform extension, which imparts distributed extension to the shallow crust. The third group represents the upper limits of viscosity and density for the deep crust; in this case the low buoyancy of the deep crust results in localized thinning of the crust with large upward motion of the Moho and lithosphere-asthenosphere boundary. These numerical experiments test the exhuming power of the deep crust in the formation of extensional gneiss domes.

1. Introduction

Flow of the deep crust is a significant mechanism for the transport of heat and mass during orogeny and is a critical geodynamic process in the chemical and physical evolution of continents. Horizontal flow is one mode of orogenic collapse (Rey et al., 2001) and may contribute to the growth of orogenic plateaus (e.g., Clark and Royden, 2000). Vertical flow in combination with horizontal flow can bring hot, deeply-sourced material to shallower levels (e.g., Burg et al., 2004; Schulmann et al., 2008; Rey et al., 2011; Teyssier and Whitney, 2002), in some cases traversing most of the thickness of the orogenic crust (Whitney et al., 2015) to within a few kilometers of the Earth's surface (Stübner et al., 2013a, 2013b; Toraman et al., 2014).

Vertical flow of hot, deep crust can create crustal-scale structures that are characterized by domal patterns of foliation in high-grade metamorphic rocks. These gneiss domes are exposed in most orogens, from Archean to Cenozoic (Teyssier and Whitney, 2002; Whitney et al., 2004, 2013). Domes are typically cored by migmatite and associated granite, which represent crystallized partial melt and magma, respectively. In many gneiss domes, the P-T paths obtained from layers and lenses of refractory lithologies included in the host quartzofeldspathic gneiss indicate isothermal decompression that was equivalent to at least 10–20 km of exhumation at high temperature (e.g., Augier et al., 2005; Bonev et al., 2005; Caby et al., 2001; de Sigoyer et al., 2004; François et al., 2014; Norlander et al., 2002; Whitney et al., 2004).

Dome formation has been previously investigated in 2D and 3D numerical modeling studies, wherein initial and/or boundary conditions were varied. Parameters varied in models include: (a) the rheology of the crust (e.g. Buck, 1991); (b) the initial geotherm (e.g. Tirel et al., 2004a; Tirel et al., 2008; Wijns et al., 2005); (c) the presence of temperature anomalies in the deep crust (e.g. Burov et al., 2014; Koptev et al., 2017); (d) the presence of partial melt in the deep crust (e.g. Rey et al., 2011; Rey et al., 2009a, 2009b; Schenker et al., 2012); (e) the presence of inherited rheological layers within the crust (e.g. Fayon et al., 2004; Huet et al., 2011; Labrousse et al., 2016; Le Pourhiet et al., 2012; Schenker et al., 2012); (f) the strength and/or presence of

* Corresponding author.
E-mail address: korch009@umn.edu (M. Korchinski).

https://doi.org/10.1016/j.tecto.2017.12.029
Received 9 May 2017; Received in revised form 27 December 2017; Accepted 29 December 2017

an initial weak zone in the crust (e.g. Fayon et al., 2004; Mezri et al., 2015); and (g) the imposed extensional velocity (e.g. Buck, 1991; Rey et al., 2011; Rey et al., 2009a, 2009b; Schenker et al., 2012; Tirel et al., 2004b; Tirel et al., 2008). We present a systematic exploration of the independent impact of the density and viscosity of the deep crust on (1) the mechanical links between the deep and shallow crust during extension, and (2) the conditions and mechanisms of deep-crust exhumation in extensional domes.

This study executed a series of 2D numerical experiments of lithospheric extension in which the viscosity and density of the deep crust were varied systematically. In order to capture the first order relationship between viscosity, strain rate and stress, we utilize a flow law that is representative of the crust to build a framework that can be used to explore the impact of compositional variances observed in nature. We used two starting crustal thicknesses (40 and 60 km), and two extensional velocities, 2 cm yr^{-1} (fast) and 2 mm yr^{-1} (slow), to evaluate the interplay among buoyancy, viscosity, and extension velocities during dome development. Numerical experiments reveal the parameter combinations that favor or suppress the generation of extensional gneiss domes, and demonstrate how the flow of deep crust is dynamically linked to strain localization or distribution in the shallow crust and the mantle.

2. Numerical experiment design

We use *Underworld*, a particle-in-cell finite element code that solves the equations for momentum, energy, and mass for incompressible flow of low Reynolds numbers (Moresi et al., 2007; Moresi et al., 2003) (Appendix A). Experiments are run using the Lithospheric Modelling Recipe: (https://github.com/OlympusMonds/lithospheric_modelling_recipe), a Python wrapper that facilitates efficient experiment design and execution. The reference experiment maps a 360 km long and 160 km deep model over a computational grid with 1 km resolution (Fig. 1). Models include from top to bottom: 10 km air layer, 20 km shallow crust (2620 $kg{\cdot}m^{-3}$), 40 km deep crust (2700–3100 $kg{\cdot}m^{-3}$), 40 km lithospheric mantle (3370 $kg{\cdot}m^{-3}$), and 50 km asthenosphere (3395 $kg{\cdot}m^{-3}$) (Fig. 1).

In the shallow crust, a 2 km-thick prism made of weaker material acts as a fault (45° dip) (Fig. 1). The fault forces deformation to localize in the center of the numerical experiment. This facilitates comparison of flow and strain patterns among the different experiments, and mitigates boundary effects (e.g., asymmetric flow) that would occur when a dome develops close to a vertical wall in the model. Similar experiments conducted by Rey et al. (2009b) tested the effect of a dipping weak prism versus a point weakness to force strain localization in the center of the experimental domain and found negligible differences. The dipping heterogeneity is preferred because it provides a geologically realistic asymmetry in the structural development of the dome (Rey et al., 2009b).

Material viscosities are temperature and strain-rate dependent, and plastic rheologies include a strain-weakening function. The visco-plastic rheology of the shallow crust is based on quartzite (Paterson and Luan, 1990), and the visco-plastic rheology of the lithospheric mantle and asthenosphere is based on wet olivine (Fig. 1; Appendix A) (Hirth and Kohlstedt, 2004). The deep crust has visco-plastic rheology based on the dry mafic granulite model of Wang et al. (2012); the starting viscosity of this layer is varied within the experiment suite.

A swarm of circular passive markers gives a qualitative representation of the finite strain field within the deep crust (Rey et al., 2009a). These markers were initially distributed as regularly spaced circles, allowing the evolution of finite strain orientations and strain intensity to be tracked within each experiment, and to be compared, at least qualitatively, across the suite of experiments. Recent 3D experiments (Rey et al., 2017) utilize similar strain markers to track finite strain in domes that develop in pull-apart systems. These 3D models show that dome material displays a double dome of foliation and a strong lineation parallel to the axis of the dome, which cannot be revealed by 2D models (see also Le Pourhiet et al., 2012). However, 2D models produce flow fields that are similar to the flow fields observed in the cross section projection of 3D models, as well as similar flow velocities, exhumation velocities, and thermal structure. Therefore, the computationally economical models presented here, although they limit strain within 2D, are nevertheless helpful for comparing flow fields within the deep crust across a wide spectrum of parameters.

The initial thermal state of each experiment is calculated using a period of thermal evolution under null extension, crustal radiogenic heating, basal heat flow, and constant surface temperature (Table 1; Appendix A). The resulting initial geotherm is characterized by a Moho temperature of ~850 °C (Fig. 1; Appendix A).

The starting reference density of deep crust is varied systematically from 2700 to 3100 $kg{\cdot}m^{-3}$ by increment of 100 $kg{\cdot}m^{-3}$. Within each experiment, density depends on temperature and melt fraction when present (see below); the coefficient of thermal expansion is kept constant across all experiments.

The reference viscosity of the deep crust is also systematically varied by changing the pre-exponential factor (A; $\eta = \frac{1}{2}\cdot A^{-1/n}\cdot\exp\left[\frac{Q}{n\cdot R\cdot T}\right]\cdot\varepsilon^{(1-n)/n}$; Appendix A) (Rey et al., 2009b, 2011). The reference viscosities are hereafter referred to as *weak* (1.0E19 Pa·s), *intermediate* (1.0E20 Pa·s), and *strong* (1.0E21 Pa·s). These values describe the viscosity at the base of the crust (immediately above Moho) at the initial time step.

The presence of melt in a dome facilitates the upward advection of heat and material (Rey et al., 2009b). In order to account for the mechanical and thermal effects of partial melting, a heuristic function is included (Rey et al., 2009a, 2009b). The melt fraction is a function of the supersolidus temperature (McKenzie and Bickle, 1988) (Appendix A). The solidus and liquidus for the crust and mantle are both temperature- and pressure-dependent and are described by polynomial functions (Fig. 1); a partial melt layer exists at the start of experiments where the geotherm crosses the solidus. The maximum partial melt fraction is 0.3, which is in line with melt fractions inferred in many gneiss (migmatite) domes (Whitney et al., 2004). The reference density of the crust decreases linearly to a maximum of 13% (Clemens and Droop, 1998), and material viscosity decreases linearly by three orders

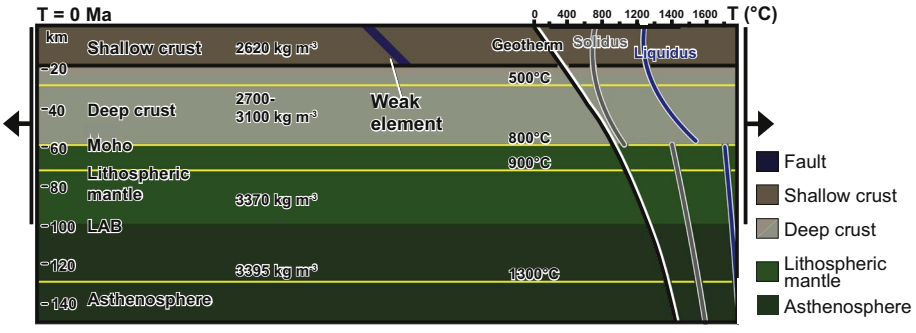

Fig. 1. Experiment input parameters, boundary conditions, and geometry. Yellow lines delineate the initial depth of isotherms. The weak element (i.e. detachment fault) is 2 km wide and is outlined in blue. The fault has the same density of the shallow crust and a Newtonian viscosity (1.0E19 Pa·s). Black arrows show applied extension velocity. LAB: lithosphere-asthenosphere boundary. (For interpretation of the references to color in this figure legend, the reader is referred to the web version of this article.)